

1  
2  
3  
4 **The delayed island mass effect: How islands can remotely**  
5 **trigger blooms in the oligotrophic ocean**  
6  
7

8 M. Messié<sup>1,2,\*</sup>, A. Petrenko<sup>1</sup>, A.M. Doglioli<sup>1</sup>, C. Aldebert<sup>1</sup>,  
9 E. Martinez<sup>3</sup>, G. Koenig<sup>1</sup>, S. Bonnet<sup>1</sup>, and T. Moutin<sup>1</sup>

10  
11 <sup>1</sup>Aix Marseille Université, Université de Toulon, CNRS, IRD, Mediterranean Institute of  
12 Oceanography (MIO), Unité Mixte 110, 13288 Marseille, France,

13 <sup>2</sup>Monterey Bay Aquarium Research Institute, Moss Landing, CA 95039, USA,

14 <sup>3</sup>University of Brest, Ifremer, CNRS, IRD, Laboratoire d'Océanographie Physique et Spatiale  
15 (LOPS), IUEM, 29200 Brest, France,

16 \*corresponding author, [monique@mbari.org](mailto:monique@mbari.org)  
17  
18  
19

20 **Key points:**

- 21 ● Previously undescribed delayed island mass effects can generate intense blooms  
22 decoupled from island fertilization both in time and in space  
23 ● These occur when diazotrophs slowly utilize excess phosphate and iron after a classical  
24 island effect while being advected away from islands  
25 ● The fertilizing impact of islands on phytoplankton may thus currently be largely  
26 underestimated in the oligotrophic ocean  
27  
28

29 **Reference:**

30 Messié, M., A. Petrenko, A. M. Doglioli, C. Aldebert, E. Martinez, G. Koenig, S. Bonnet, and T. Moutin  
31 (2020). The Delayed Island Mass Effect: how islands can remotely trigger blooms in the oligotrophic  
32 ocean. *Geophysical Research Letters*, in press, <https://doi.org/10.1029/2019GL085282>

33 **Abstract**

34 In oligotrophic gyres of the tropical ocean, islands can enhance phytoplankton biomass and  
35 create hotspots of productivity and biodiversity. This “Island Mass Effect” (IME) is typically  
36 identified by increased chlorophyll concentrations next to an island. Here we use a simple  
37 plankton model in a Lagrangian framework to represent an unexplained open ocean bloom,  
38 demonstrating how islands could have triggered it remotely. This new type of IME, termed  
39 “delayed IME”, occurs when nitrate is limiting, N:P ratios are low, and excess phosphate and  
40 iron remain in water masses after an initial bloom associated with a “classical” IME. Nitrogen  
41 fixers then slowly utilize leftover phosphate and iron while water masses get advected away,  
42 resulting in a bloom decoupled in time (several weeks) and space (hundreds of km) from island-  
43 driven nutrient supply. This study suggests that the fertilizing effect of islands on phytoplankton  
44 may have been largely underestimated.

45

46 **Plain language summary**

47 In the poor and nutrient-depleted waters of the tropical Pacific, islands act as sources of nutrients  
48 fertilizing nearby waters. These nutrients are consumed by microscopic photosynthesizing algae,  
49 the phytoplankton. The resulting phytoplankton enrichments (blooms) in turn support productive  
50 ecosystems. This phenomenon, termed the “island mass effect”, has been known for sixty years  
51 and is classically defined by increased chlorophyll (representing phytoplankton biomass) next to  
52 an island. Blooms also occur in the open ocean and are usually attributed to vertical processes  
53 such as mixing or uplifting that locally supply nutrients from subsurface reservoirs. In this paper,  
54 we demonstrate that a different type of island mass effect exists, where the phytoplankton  
55 response is delayed because they grow very slowly. These blooms are supported by the nitrogen  
56 fixer *Trichodesmium*. Since phytoplankton get carried away from islands by oceanic currents  
57 while they grow, this can lead to a bloom located hundreds of km away with no apparent  
58 connection to the islands. Nutrient inputs by islands followed by advection can thus trigger  
59 remote blooms in the open ocean. Our study suggests that the fertilizing effect of islands may  
60 currently be largely underestimated, particularly in the warm waters of the tropical Pacific where  
61 *Trichodesmium* is common.

62

63

64 **Index terms**

- 65 4855 Phytoplankton
- 66 4815 Ecosystems, structure, dynamics, and modeling (0439)
- 67 4845 Nutrients and nutrient cycling (0470, 1050)
- 68 4512 Currents
- 69 4562 Topographic/bathymetric interactions

70

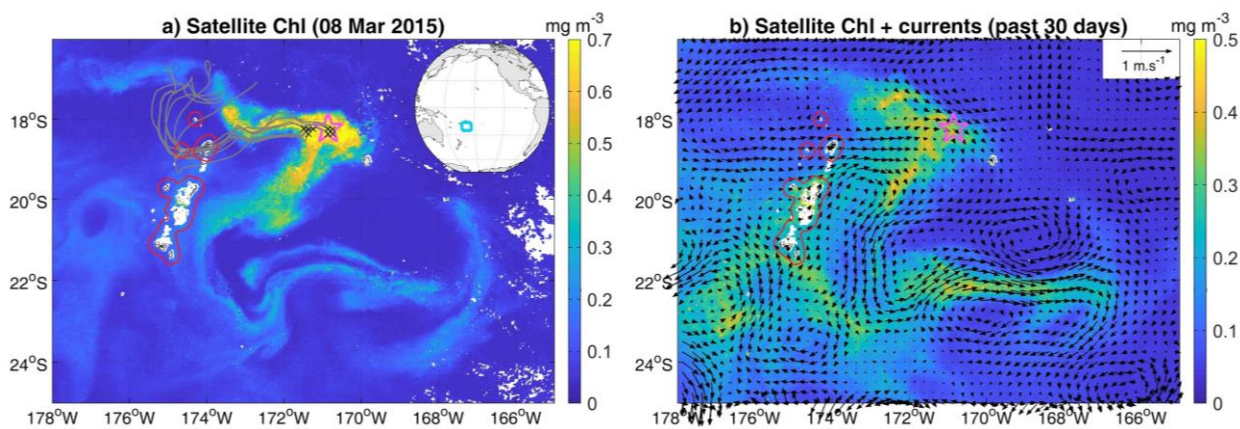
71 **Keywords:** island mass effect, nitrogen fixation, Lagrangian analysis, phytoplankton bloom,  
72 oligotrophic ocean, nutrient supply

73

74 **1. Introduction**

75 In the mostly oligotrophic tropical ocean, phytoplankton blooms sometimes do occur,  
 76 dramatically increasing local production (Behrenfeld & Boss, 2014; Messié et al., 2006; Ryan et  
 77 al., 2002; Wilson & Qiu, 2008; Wilson et al., 2008). These blooms are triggered by an unusual  
 78 supply of nutrients often resulting from short-lived vertical transport (Johnson et al., 2010;  
 79 Wilson & Qiu, 2008) driven by (sub)mesoscale oceanic circulation (Mahadevan, 2016; Ryan et  
 80 al., 2002), winds (Menkes et al., 2016) or a combination of both (McGillicuddy et al., 2007).  
 81 Additional processes initiating and enhancing blooms include vertically migrating phytoplankton  
 82 (Wilson et al., 2008), dispersion/dilution (Lehahn et al., 2017), seasonal mixing followed by  
 83 stratification (Dore et al., 2008; Moutin et al., 2018), and island-driven nutrient supply (Gove et  
 84 al., 2016; Wilson & Qiu, 2008).

85 The fertilizing effect of islands on oceanic productivity has been known for decades. Termed the  
 86 Island Mass Effect (IME) by Doty and Oguri (1956), this process is almost ubiquitous across the  
 87 tropical Pacific (Gove et al., 2016). In its classical sense, the IME is characterized by an inverse  
 88 relationship between distance to an island and phytoplankton biomass and/or productivity, often  
 89 represented by surface chlorophyll concentration (Chl). Biological enrichments are not always  
 90 confined near the islands; Chl can peak downstream when lee eddies form (Hasegawa et al.,  
 91 2009; Messié et al., 2006) and Chl enrichments can be spread by currents over hundreds of km  
 92 (Shiozaki et al., 2014; Signorini et al., 1999). However, including in these cases, IMEs described  
 93 in the literature (hereafter “classical IMEs”) always remain characterized by increased Chl  
 94 spatially connected to an island.



95 **Figure 1:** Satellite-derived contextual information. The Tonga islands are visible near  $175^\circ\text{W}$ ; the region  
 96 within 15 km of Tonga major coastlines is contoured in red. The pink star represents station LD-B  
 97 occupied during March 15-20, 2015. a) Chl observed at the peak of the LD-B bloom. Reproducing  
 98 previous results (de Verneil et al., 2017; Rousselet et al., 2018), grey lines display 60-day backward  
 99 Lagrangian trajectories initialized at high-Chl patches near LD-B ( $\text{Chl} > 0.75 \text{ mg m}^{-3}$ , black crosses). b)  
 100 Chl and surface currents observed during the previous 30 days, providing information on water mass  
 101 pathway and bloom generation (note the different colorbar).  
 102

103 In this context, a spectacular bloom observed from space in the western tropical South Pacific  
 104 early 2015 is puzzling (Fig. 1). The bloom occurred during the Oligotrophy to UTRa-oligotrophy  
 105 PACific Experiment (OUTPACE) oceanographic cruise (Moutin et al., 2017), and was targeted  
 106 by a Long Duration station (LD-B) due to its unusually high Chl for the region ( $> 0.9 \text{ mg m}^{-3}$ ). In  
 107 order to study fine-scale physical-biological coupling, high resolution measurements were

108 performed when the vessel reached the bloom a week after its satellite-detected peak.  
109 Surprisingly, physical data revealed a stratified water column with no evidence of mixing,  
110 upwelling or submesoscale activity (de Verneil et al., 2017). At the same time, shipboard  $^{15}\text{N}_2$   
111 isotopic measurements unveiled very high nitrogen fixation rates sustaining nearly all new  
112 primary production (Caffin et al., 2018a), mostly supported by the diazotroph *Trichodesmium*  
113 (Bonnet et al., 2018). While nitrogen fixation is common in the region (Bonnet et al., 2017,  
114 2018; Shiozaki et al., 2014), the process responsible for supplying enough nutrients to support  
115 this remarkably high biological production is unclear. High-phosphate waters had been advected  
116 from the eastern gyre (Bonnet et al., 2017), but the origin of iron remained a mystery, especially  
117 since diazotrophs need considerably more iron than non-diazotrophic phytoplankton (Berman-  
118 Frank et al., 2001). Local stratification ruled out vertical transport or mixing, and atmospheric  
119 deposition was low (Guieu et al., 2018). The only plausible hypothesis was offered by de Verneil  
120 et al. (2017), who suggested that iron was provided by an island contact. Indeed, although  
121 traveling on average westward, the eastern gyre waters passed near the Tonga islands early  
122 February, before they recirculated eastward toward LD-B (Fig. 1, grey).

123 In contrast to previous reports of island-driven *Trichodesmium* blooms (Shiozaki et al., 2014),  
124 however, the LD-B bloom is clearly disconnected from the Tonga islands (Fig. 1). The classical  
125 IME definition thus does not apply, and whether the bloom was triggered by islands remains to  
126 be demonstrated. We propose that the LD-B bloom is an undescribed type of IME, termed  
127 “delayed IME”, where the phytoplankton respond so slowly to island fertilization that the bloom  
128 becomes separated from the islands as water masses are advected away. This hypothesis was  
129 tested first by investigating a potential nutrient release by the Tonga islands, and then by  
130 modeling the LD-B bloom using exclusively an island nutrient source and surface advection. Our  
131 simulations demonstrate how the Tonga islands could have indeed triggered the bloom, and  
132 provide a proof of concept for the existence of the delayed IME.

## 133 2. Materials and methods

### 134 2.1. Datasets and Lagrangian analysis

135 Satellite-derived surface Chl and currents were produced specifically for OUTPACE by  
136 Ssalto/Duacs and CLS with support from TOSCA/CNES. A complete description and validation  
137 can be found in de Verneil et al. (2017) and Rousselet et al. (2018). Briefly, surface Chl  
138 (available December 2<sup>nd</sup>, 2014 to May 10<sup>th</sup>, 2015, 1/50° daily) were obtained from  
139 Suomi/NPP/VIIRS measurements and computed as 5-day weighted averages; resulting  
140 concentrations agree well with *in situ* underway Chl (Rousselet et al., 2018). Surface currents  
141 (1/8° daily) combine absolute geostrophic velocities, wind-induced Ekman circulation relative to  
142 15 m, and a cyclogeostrophy correction. These custom products provide higher spatial and  
143 temporal resolution, and better quality, than the typically available global products. Following  
144 Gove et al. (2016), shallow pixels were removed as they were potentially contaminated by  
145 bottom reflectance (white pixels near Tonga in Fig. 1: minimum depth < 30m according to  
146 ETOPO1 bathymetry, extended by one additional pixel in all directions). Precipitation was  
147 obtained from the Global Precipitation Measurement project (GPM IMERG v06, 0.1° daily,  
148 Huffman et al., 2019).

149 Ninety-day forward and backward Lagrangian trajectories, initialized at the center of each of the  
 150 83 current pixels located within 15 km of the major Tonga coastlines (15-km Tonga region, red  
 151 contour in Fig. 1), were computed for each of the 160 days of the Chl time period. The  
 152 Lagrangian diagnostic tool Ariane was used (Blanke & Raynaud, 1997), with a time step of 0.1  
 153 day. East/west water mass origin was defined for each pixel as the mean longitude during the  
 154 previous 90 days minus the pixel longitude, as eastern waters are likely phosphate-rich (Bonnet  
 155 et al., 2017; Moutin et al., 2008). Along-trajectory Chl was obtained by spatially interpolating  
 156 smoothed Chl maps from the nearest day, generated to minimize data noise and gaps due to  
 157 clouds using 2 iterations of spatial median filtering followed by a temporal linear interpolation of  
 158 gaps not exceeding 5 days. For each trajectory, the average Chl 5-10 days upstream was termed  
 159 Chl<sub>upstream</sub>, and the Chl increase when passing by the islands was defined as  $\Delta\text{Chl} = \text{Chl}(0) -$   
 160 Chl<sub>upstream</sub> (see Fig. S1).

## 161 2.2. The growth-advection approach

162 A simple plankton model was used, representing three nutrients (nitrogen N, phosphate P, and  
 163 iron Fe), two phytoplankton (non-diazotrophic phytoplankton *Phy* and *Trichodesmium Tri*), and  
 164 one zooplankton (*Z*) (Text S1, Fig. S2). Beyond its N<sub>2</sub>-fixing capability, *Tri* differs from *Phy* by  
 165 its much slower maximum growth rate (0.27 d<sup>-1</sup> vs. 1 d<sup>-1</sup>) and its closure term (grazing for *Phy*  
 166 vs. death for *Tri*, see details in Text S1). *Tri* death includes a programmed cell death (PCD),  
 167 likely responsible for the LD-B bloom demise (Spungin et al., 2018), by which *Trichodesmium*  
 168 blooms can collapse in a few days in response to nutrient stress (Berman-Frank et al., 2004).  
 169 Modeled Chl follows assumed C:Chl ratios for *Phy* and *Tri*. The full model description,  
 170 equations and parameters are given in Text S1 and Table S1.

171 The plankton model was coupled to island-driven nutrient supply and oceanic advection using a  
 172 “growth-advection” method developed off California (Messié & Chavez, 2017). The method  
 173 considers the evolution of plankton communities within the surface mixed layer of a water mass,  
 174 as triggered by a fertilization process (here the IME) and advected by surface currents.  
 175 Concretely, plankton biomass is simulated over time following an initial input of nutrients, and  
 176 mapped on Lagrangian trajectories. Initial conditions constrain the intensity and timing of the  
 177 Chl peaks and surface currents dictate their location.

178 Daily simulations were initialized within the 15-km Tonga region at the same locations as  
 179 Lagrangian trajectories, with initial plankton concentrations constrained by Chl<sub>upstream</sub> (Text  
 180 S1). Initial nutrient concentrations N(0), P(0), and Fe(0) represent island-driven nutrient supply  
 181 plus upstream concentrations (only for P). Because N-limited *Phy* grows faster and drives the  
 182 initial bloom, N(0) was set proportional to  $\Delta\text{Chl}$ . P(0) was proportional to N(0) in Redfield  
 183 proportions, with an additional P source when water masses originated from the east. Finally, the  
 184 Tonga islands being volcanic, the island bedrock and/or sediments are likely iron-rich and can  
 185 represent a significant source of iron (Palacios, 2002; Blain et al., 2008; Raapoto et al., 2019).  
 186 Submarine groundwater discharge may also release iron, particularly for small tropical islands  
 187 like Tonga (Moosdorf et al., 2015). Past studies found links between IMEs and surface currents  
 188 with no evidence of upwelling, and proposed that turbulent mixing entrains iron-rich waters  
 189 (Signorini et al., 1999; Martinez & Maamaatuaiahutapu, 2004). Fe(0) was thus proportional to  
 190 current speed. All initialization parameters are given in Table S2.

191 Daily runs were computed from December 2<sup>nd</sup>, 2014 to April 15<sup>th</sup>, 2015 by mapping 90-day  
 192 plankton model output initialized daily onto the corresponding forward Lagrangian trajectory.

193 Horizontal and vertical mixing was neglected (see Messié & Chavez (2017) for more details on  
194 the method). The daily runs were then combined into  $1/8^\circ$  daily gridded maps by keeping, for  
195 each day and each pixel, the maximum value from all runs. The maximum rather than the mean  
196 was used to avoid unrealistic dilution by low-Chl trajectories. A 5-day weighted average was  
197 then computed, following the method applied to satellite Chl.

### 198 2.3. Model optimization

199 The model solution depends on a number of constants, used to parameterize the plankton model  
200 and its initialization (Tables S1 and S2). Most of the plankton model parameters were obtained  
201 from the literature and/or from OUTPACE measurements. Some parameters were unknown  
202 either because of a process never having been modeled before, namely the PCD, or because no  
203 data was available to constrain them, such as parameters controlling initialization in the island  
204 vicinity (which was not sampled during OUTPACE). These parameters were first manually  
205 roughly tuned so that the model approximately represented satellite Chl. The corresponding  
206 model solution reproduced the major Chl blooms, although their timing was off by a few days  
207 (Fig. S3). Then, the parameters were fine-tuned using a gradient-based optimization method in  
208 order to best fit observations of satellite Chl (Text S2). The method optimized a cost function  
209 based on RMS differences of modeled and satellite Chl in delayed IME regions; classical IMEs  
210 were thus not optimized and were overestimated (Fig. S3). Details on the cost function, the  
211 optimization method and its results are provided in Text S2 and Fig. S3.

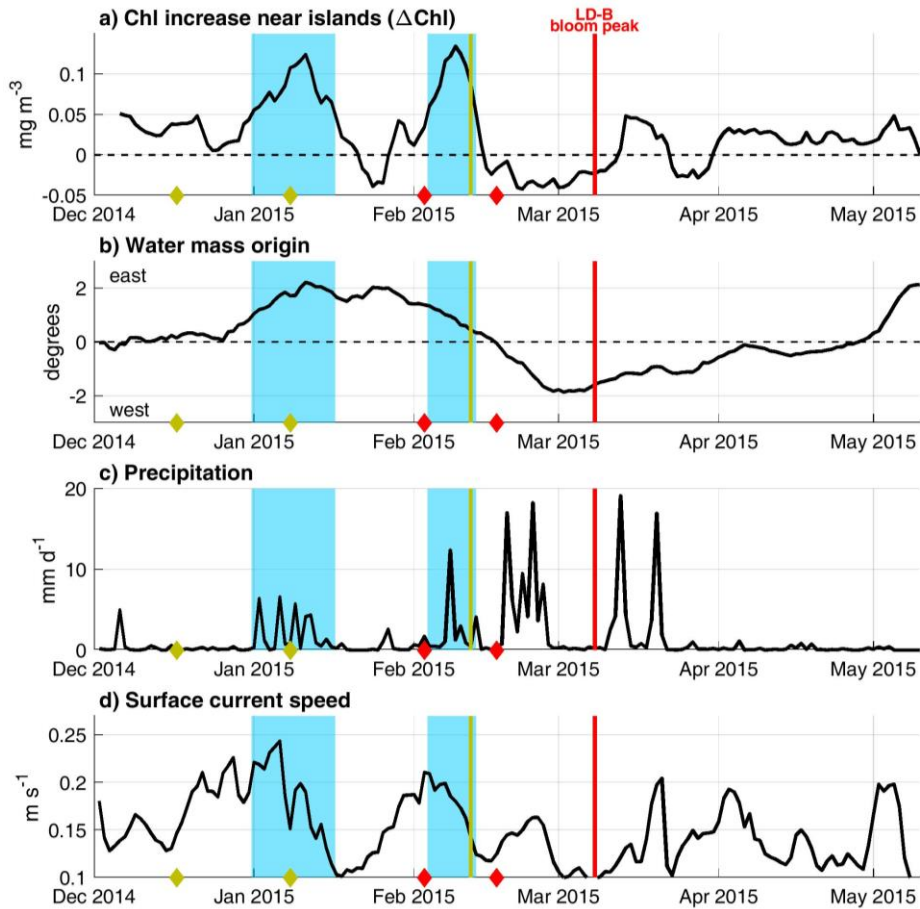
## 212 3. Results and discussion

### 213 3.1. Island-driven nutrient supply

214 A significant satellite Chl increase when passing by the islands ( $\Delta\text{Chl}$ ) reveals an island-driven  
215 supply of nutrients supporting a classical IME. Two high- $\Delta\text{Chl}$  events were observed during the  
216 period of study (Fig. 2a, blue shading), indicating that the Tonga islands can effectively act as a  
217 nutrient source. At the peak of both events (January 11<sup>th</sup> and February 9<sup>th</sup>, 2015),  $\Delta\text{Chl}$   
218 represented a  $> 90\%$  increase relative to upstream Chl. The eastern origin of water masses during  
219 both events (Fig. 2b) indicates that waters were likely phosphate-rich but nitrate- and iron-  
220 depleted (Bonnet et al., 2017; Moutin et al., 2008). Islands must have thus supplied at least  
221 nitrate and/or iron to support the Chl increase.

222 Islands can supply nutrients through several processes, including wind-driven coastal upwelling,  
223 uplifting and mixing in lee eddies, land runoff, atoll lagoon flushing, coral reef benthic  
224 processes, and iron enrichment from the island platform (Gove et al., 2016; Hasegawa et al.,  
225 2009; Palacios 2002; Signorini et al., 1999). No correspondence was found between  $\Delta\text{Chl}$  and  
226 sea surface temperature, waves, or tides, so upwelling and lagoon flushing were unlikely. Island  
227 runoff was a possibility since both classical IMEs coincided with precipitation events (Fig. 2c).  
228 The Tonga islands considered here (part of the Vava'u and Ha'apai groups) are mostly low  
229 volcanic coral islands, but Vava'u slopes up to 200m-high cliffs in the north and rain could  
230 trigger significant runoff. However, not all precipitation events coincided with a Chl increase  
231 near the islands. Precipitation may thus be a necessary, but not sufficient, condition to trigger a  
232 classical IME. Surface currents and  $\Delta\text{Chl}$  are significantly correlated ( $r = 0.56$  with a lag of 4-6

233 days,  $p < 0.01$ ), and delayed bloom water mass origin coincides with strong currents (Fig. 2d  
 234 diamonds), supporting the hypothesis of an additional iron source related to currents.

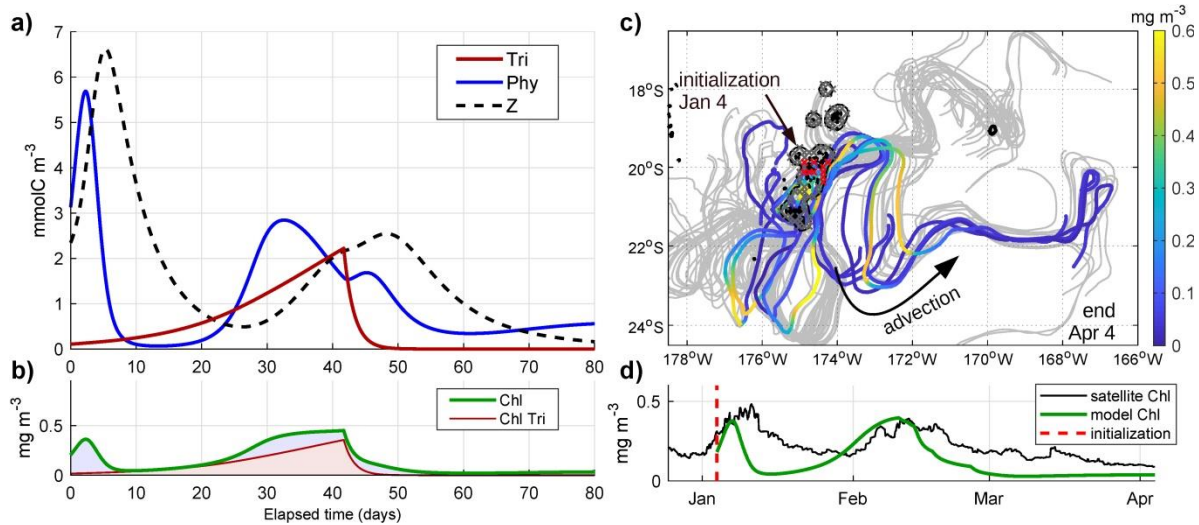


235  
 236 **Figure 2:** Characterization of the Tonga classical IME and its potential drivers. All variables were averaged over  
 237 the 15-km Tonga region. Blue shading highlight times of significant Chl increase near islands, defined as  $\Delta\text{Chl} >$   
 238  $0.05 \text{ mg m}^{-3}$ . The red line marks the LD-B bloom peak, and red diamonds circumscribe the period when 80% of its  
 239 island-origin water masses\* traveled through the 15-km Tonga region (\*defined as along-trajectory satellite Chl  $>$   
 240  $0.7 \text{ mg m}^{-3}$  within 2 days of the bloom peak in the LD-B region, Fig. S3). Dark yellow similarly displays the delayed  
 241 SW bloom peak and origin (see section 3.3).

242 **3.2. Biological evolution following island fertilization**

243 The temporal evolution of satellite Chl downstream of Tonga along the Lagrangian trajectories  
 244 (Fig. S1) clearly displays the classical IME in a significant number of trajectories, peaking within  
 245 a few days. Interestingly, Chl usually displayed a second, separate peak weeks later. No  
 246 significant water mass cooling was observed, so additional vertical nutrient inputs were unlikely.  
 247 We propose that the two successive plankton blooms were supported by the same island-driven  
 248 nutrient supply, indicating that two phytoplankton types responded to island fertilization with  
 249 different time lags. *Trichodesmium* grow slower than most phytoplankton (Capone et al., 1997)  
 250 and were thus likely responsible for the second bloom (delayed IME), as observed at LD-B  
 251 (Bonnet et al., 2018). The first bloom (classical IME) was likely supported by non-diazotrophic  
 252 phytoplankton, because another diazotroph species would have consumed all available phosphate  
 253 and iron, preventing the delayed bloom from occurring.





254

255 **Figure 3:** Example of plankton model output (left) and growth-advection run initialized on January 4<sup>th</sup>,  
 256 2015 (right). a) Modeled plankton biomass as a function of time, following initialization corresponding to  
 257 median conditions at the red crosses in c). b) Corresponding modeled Chl, total (green line) and of Tri  
 258 (dark red line). Both the intensity and timing of the two Chl peaks depend on initial conditions. c) Ninety-  
 259 day forward trajectories (grey or color) initialized at grey and red crosses near the Tonga islands. Along-  
 260 trajectory modeled Chl is displayed in color for a few example trajectories initialized at the red crosses  
 261 (between 19-20.5°S for  $\Delta\text{Chl} > 0.05 \text{ mg m}^{-3}$  and currents  $> 0.2 \text{ m s}^{-1}$ ). d) Time series of modeled (green)  
 262 and observed (black) along-trajectory Chl, averaged for the example trajectories. The shape of the  
 263 modeled delayed Chl peak is different in d than b, because its timing differs across the trajectories being  
 264 averaged in d due to varying initial conditions. See Text S1 and S2 regarding underestimated Chl in non-  
 265 bloom conditions.

266 The plankton model was used to represent the temporal evolution of non-diazotrophic  
 267 phytoplankton (*Phy*) and *Trichodesmium* (*Tri*) after an initial supply of nutrients (Fig. 3a,b). The  
 268 model represents a classical IME paradigm where *Phy* blooms within a few days. Nitrate  
 269 exhaustion and predation terminate this early bloom after about one week. The model  
 270 additionally predicts a separate, *Tri*-dominated later peak: the delayed IME. It occurs because *Tri*  
 271 grows slowly and utilizes leftover phosphate and iron over several weeks. A secondary *Phy* peak  
 272 is also observed around the *Tri* maximum, supported by nutrients released by *Tri* that, in turn,  
 273 enhance the bloom. Similar biological production enhancements due to *Trichodesmium* nutrient  
 274 release have been observed previously (Bonnet et al., 2016; Caffin et al., 2018b). Once  
 275 phosphate and/or iron stress become too high, the PCD causes the *Tri* bloom to collapse.

276 When considering advection by surface currents, the early and late Chl maxima translate into a  
 277 peak near the islands (classical IME) and peaks in several locations away from the islands  
 278 (delayed IME), respectively (Fig. 3c). Not all trajectories display both an early and late Chl peak,  
 279 consistent with satellite observations (Fig. S1). This is because *Phy* and *Tri* are decoupled in the  
 280 model, *Phy* being primarily a function of  $\Delta\text{Chl}$  (controlling N(0)) and *Tri* of currents and water  
 281 mass origin (controlling Fe(0) and excess P relative to N, respectively). The modeled Chl peak  
 282 timing is close to the timing of early and late peaks observed in satellite along-trajectory Chl  
 283 (Fig. 3d). *Tri*'s slow growth rate is thus responsible for the temporal decoupling between island  
 284 fertilization and delayed IME, while advection by surface currents explains their spatial  
 285 decoupling.



## 286 3.3. Classical and delayed IME impacts on phytoplankton

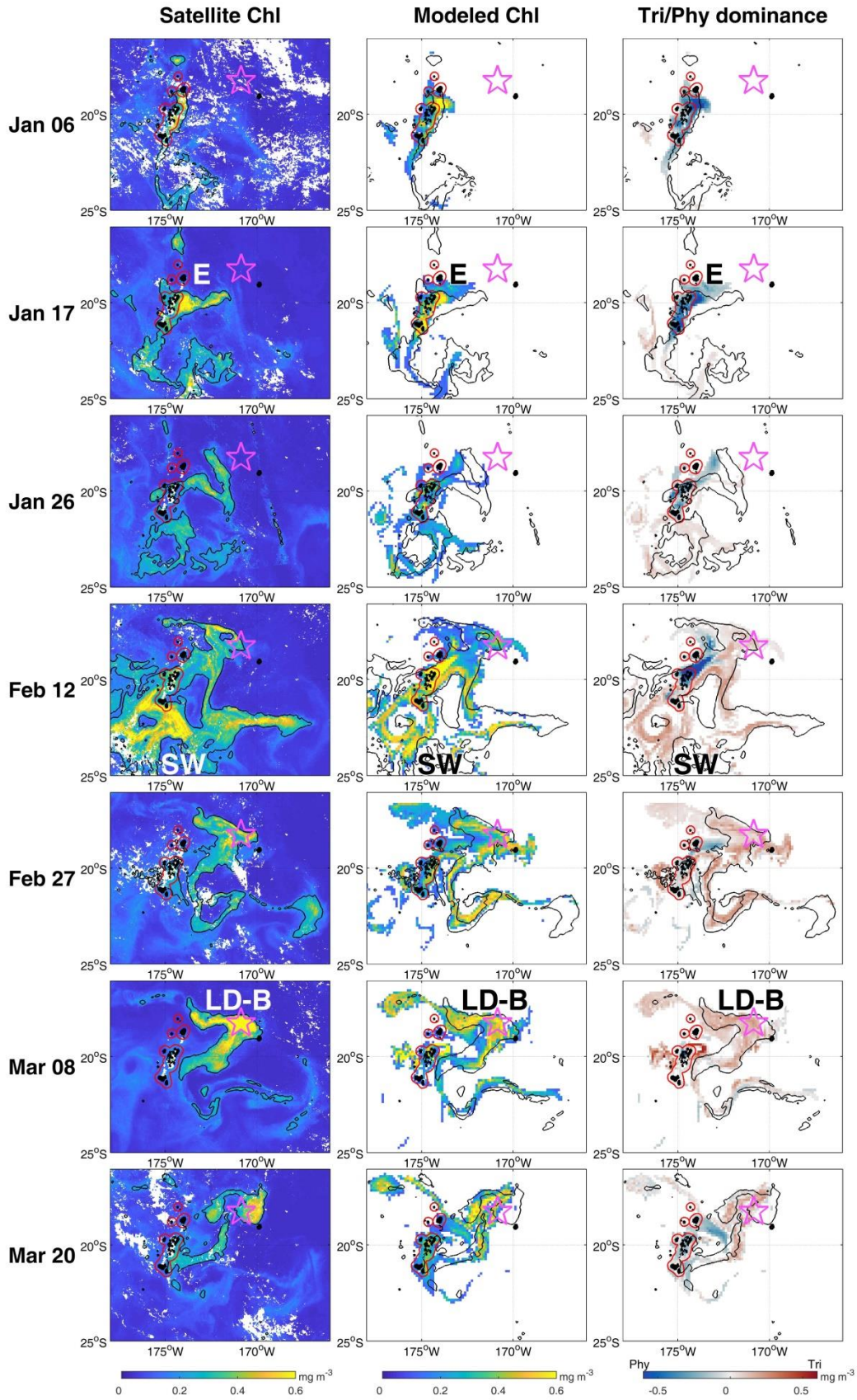
287 Time-varying satellite Chl maps highlight several major blooms during the period of study (Fig.  
288 4, see also Movie S1): east (E) bloom close to Tonga in January, southwest (SW) bloom  
289 downstream of Tonga in mid-February, and LD-B bloom early March. These are separate from  
290 near-island Chl increases depicted in Fig. 2 (blue shading). Island-driven Chl enrichments were  
291 examined by combining individual growth-advection daily runs (e.g., Fig. 3c) into gridded daily  
292 maps. The result is remarkably similar to satellite Chl (Fig. 3d, 4 and Fig. S3), requiring only  
293 island fertilization and oceanic advection to reproduce major bloom timing and spatial features.  
294 Using the *Tri-Phy* dominance as an indicator of delayed vs. classical IME, the model identifies  
295 the E bloom as a classical IME and the SW and LD-B blooms as delayed IMEs. These represent  
296 two different situations: the SW bloom remained connected to the islands as water masses  
297 recirculated towards Tonga, while the LD-B bloom became separated as water masses got  
298 advected away. Both were preceded by island-driven fertilization and a classical IME by about  
299 one month (Fig. 2a).

300 The model's success in representing satellite Chl has two implications. First, island-driven  
301 nutrient supply and oceanic advection are sufficient to reproduce the LD-B bloom, supporting  
302 the hypothesis that the bloom was a delayed IME fertilized by the Tonga islands. Second, the  
303 growth-advection model represents all satellite-detected blooms, indicating that they were likely  
304 triggered by island effects. This suggests that islands were not only responsible for the LD-B  
305 bloom, but even more remarkably were the primary driver of Chl variability in the region for the  
306 period of study. Island-driven iron inputs, in addition to submarine hydrothermal iron sources  
307 (Guieu et al., 2018), may thus contribute to explain the hotspot of nitrogen fixation found in the  
308 western tropical South Pacific (Bonnet et al., 2017). Indeed, top 30m iron concentrations along  
309 the OUTPACE transect were highest around the Tonga islands ( $0.98 \pm 0.16$  nM), an area where  
310 deeper concentrations were relatively low ( $0.59 \pm 0.21$  nM) (Guieu et al., 2018).

311 The prevalence of delayed IMEs is difficult to quantify beyond the region and period of study. A  
312 detailed Lagrangian analysis, as performed here, would be needed to determine if an open-ocean  
313 bloom was fueled by island effects or by local processes. Our analysis required daily high-  
314 resolution Chl and current satellite products, that were specifically produced for OUTPACE and  
315 are unfortunately not available on a regular basis. Nevertheless, an analysis of VIIRS chlorophyll  
316 near Tonga does suggest that delayed IMEs may be common in the region, particularly in  
317 summer (Fig. S4). More generally, delayed IMEs may occur when conditions support  
318 diazotrophy (warm temperatures and stratified waters) in the presence of islands supplying iron  
319 and/or phosphate. Regions such as Melanesia's eastern boundary (i.e., Fiji and Tonga islands)  
320 appear particularly favorable, as westbound phosphate-rich waters intersect volcanic, iron-rich  
321 islands.

322 Regardless of their frequency, delayed IMEs can be responsible for unusually strong  
323 phytoplankton blooms in a largely oligotrophic environment. At the peak of the two delayed  
324 IMEs described here, Chl reached values close to  $1 \text{ mg m}^{-3}$ , a tenfold increase relative to  
325 background concentrations. While classical IMEs can reach similar concentrations, the duration  
326 and spatial extent of delayed IMEs were much higher in the model (Fig. 3, 4). Summing the  
327 corresponding modeled Chl over space and time, delayed IMEs were responsible for enrichments  
328 ( $> 0.1 \text{ mg m}^{-3}$ ) over twice as high as those of classical IMEs, even though classical IMEs were  
329 overestimated (Fig. S3).

The delayed island mass effect



331 **Figure 4:** *Chl temporal evolution as observed from satellite and modeled using the growth-advection*  
 332 *method (see also Movie S1). Left: daily satellite Chl. Middle: model output, keeping only pixels where*  
 333 *modeled Chl > 0.1 mg m<sup>-3</sup>. Right: Tri-Phy dominance defined as Tri Chl minus Phy Chl, also*  
 334 *representing the classical (Phy-dominated, blue) vs. delayed (Tri-dominated, red) IMEs. In all panels,*  
 335 *black contours represent the 0.2 mg m<sup>-3</sup> Chl contour from the satellite smoothed product, red contours*  
 336 *encircle the 15-km Tonga region, and the pink star is the LD-B location.*

#### 337 **4. Conclusion**

338 This study provides strong evidence for the existence of delayed IMEs, a previously undescribed  
 339 type of island effect where the bloom is spatially and temporally decoupled from island  
 340 fertilization. Contrary to classical IMEs where phytoplankton respond quickly, resulting in a  
 341 bloom near an island, delayed IMEs are supported by slow-growing nitrogen fixers such as  
 342 *Trichodesmium*. They can occur when conditions are favorable for diazotrophy (e.g., warm  
 343 stratified waters) and excess iron and phosphate remain in water masses after a classical IME.

344 Delayed IMEs represent situations where the time scale for biology (weeks) is much longer than  
 345 the advection time scale (days), which is very unusual in the ocean and results in a temporal and  
 346 spatial decoupling between nutrient supply processes and phytoplankton response. Such a  
 347 mismatch between biological and physical time scales can lead to unexpected blooms in  
 348 stratified waters with no apparent origin. In particular, delayed IMEs do not match the classical  
 349 IME definition of Chl increase nearby islands and would not be identified by traditional IME  
 350 detection methods such as a Chl contour (Shiozaki et al., 2014) or an inverse relationship  
 351 between Chl and distance to an island (Gove et al., 2016). Without *in situ* subsurface data  
 352 revealing the lack of vertical processes, these remote blooms could be mistakenly attributed to  
 353 (sub)mesoscale activity. Island effects on phytoplankton biomass and productivity may thus have  
 354 been largely underestimated.

#### 355 **Acknowledgements and data**

356 M.M. was funded by the European Union's Horizon 2020 research and innovation programme  
 357 under the Marie Skłodowska-Curie grant agreement SAPPHERE No. 746530. This research is a  
 358 contribution of the OUTPACE project (<http://doi.org/10.17600/15000900>), funded by the  
 359 Agence Nationale de la Recherche (ANR-14-CE01-0007-01), the LEFE-CyBER program  
 360 (CNRS-INSU), the Institut de Recherche pour le Développement (IRD), the GOPS program  
 361 (IRD) and TOSCA/CNES (BC T23, ZBC 4500048836). The growth-advection method was  
 362 developed under NASA grant 80NSSC17K0574, and the optimization method under French  
 363 ANR/DGA project Turbidant (ANR16-ASTR-0019-01). We thank Louise Rousselet and  
 364 Stéphanie Barrillon for their help with Ariane, Isabelle Pujol and Guillaume Taburet (CLS) for  
 365 their support with satellite-derived products, and Eric Pape for useful comments and text edits.  
 366 Satellite chlorophyll and currents are available at [http://www.obs-](http://www.obs-vlfr.fr/proof/php/outpace/outpace_data.php)  
 367 [vlfr.fr/proof/php/outpace/outpace\\_data.php](http://www.obs-vlfr.fr/proof/php/outpace/outpace_data.php), and precipitation at  
 368 [https://disc.gsfc.nasa.gov/datasets/GPM\\_3IMERGDF\\_V06/summary](https://disc.gsfc.nasa.gov/datasets/GPM_3IMERGDF_V06/summary).  
 369

370 **References**

- 371 Behrenfeld, M. J., & Boss, E. S. (2014), Resurrecting the ecological underpinnings of ocean plankton  
372 blooms, *Ann. Rev. Mar. Sci.*, 6, 167-194, <https://doi.org/10.1146/annurev-marine-052913-021325>
- 373 Berman-Frank, I., Cullen, J. T., Shaked, Y., Sherrell, R. M., & Falkowski, P. G. (2001), Iron availability,  
374 cellular iron quotas, and nitrogen fixation in *Trichodesmium*, *Limnol. Oceanogr.*, 46(6), 1249-1260,  
375 <https://doi.org/10.4319/lo.2001.46.6.1249>
- 376 Berman-Frank, I., Bidle, K., Haramaty, L., & Falkowski, P. G. (2004), The demise of the marine  
377 cyanobacterium, *Trichodesmium* spp., via an autocatalyzed cell death pathway, *Limnol. Oceanogr.*,  
378 49, 997-1005, <https://doi.org/10.4319/lo.2004.49.4.0997>
- 379 Blain, S., Sarthou, G., & Laan, P. (2008), Distribution of dissolved iron during the natural iron-  
380 fertilization experiment KEOPS (Kerguelen Plateau, Southern Ocean), *Deep Sea Res. Part II*, 55(5-7),  
381 594-605, <https://doi.org/10.1016/j.dsr2.2007.12.028>
- 382 Blanke, B., & Raynaud, S. (1997), Kinematics of the Pacific Equatorial Undercurrent: an Eulerian and  
383 Lagrangian approach from GCM results, *J. Phys. Oceanogr.*, 27(6), 1038-1053,  
384 [https://doi.org/10.1175/1520-0485\(1997\)027<1038:KOTPEU>2.0.CO;2](https://doi.org/10.1175/1520-0485(1997)027<1038:KOTPEU>2.0.CO;2)
- 385 Bonnet, S., Berthelot, H., Turk-Kubo, K., Cornet-Barthaux, V., Fawcett, S., Berman-Frank, I., et al.  
386 (2016), Diazotroph derived nitrogen supports diatom growth in the South West Pacific: A quantitative  
387 study using nanoSIMS, *Limnol. Oceanogr.*, 61(5), 1549-1562, <https://doi.org/10.1002/lno.10300>
- 388 Bonnet, S., Caffin, M., Berthelot, H., Grosso, O., Benavides, M., Helias-Nunige, S., et al. (2018), In-  
389 depth characterization of diazotroph activity across the western tropical South Pacific hotspot of N<sub>2</sub>  
390 fixation (OUTPACE cruise), *Biogeosciences*, 15(13), 4215-4232, [https://doi.org/10.5194/bg-15-4215-](https://doi.org/10.5194/bg-15-4215-2018)  
391 2018
- 392 Bonnet, S., Caffin, M., Berthelot, H., & Moutin, T. (2017), Hot spot of N<sub>2</sub> fixation in the western tropical  
393 South Pacific pleads for a spatial decoupling between N<sub>2</sub> fixation and denitrification, *Proc. Natl.*  
394 *Acad. Sci.*, 114(14), E2800-E2801, <https://doi.org/10.1073/pnas.1619514114>
- 395 Caffin, M., Berthelot, H., Cornet-Barthaux, V., Barani, A., & S. Bonnet, S. (2018b), Transfer of  
396 diazotroph-derived nitrogen to the planktonic food web across gradients of N<sub>2</sub> fixation activity and  
397 diversity in the western tropical South Pacific Ocean, *Biogeosciences*, 15(12), 3795-3810,  
398 <https://doi.org/10.5194/bg-15-3795-2018>
- 399 Caffin, M., Moutin, T., Foster, R. A., Bouruet-Aubertot, P., Doglioli, A. M., Berthelot, H., et al. (2018a),  
400 N<sub>2</sub> fixation as a dominant new N source in the western tropical South Pacific Ocean (OUTPACE  
401 cruise), *Biogeosciences*, 15(8), 2565-2585, <https://doi.org/10.5194/bg-15-2565-2018>
- 402 Capone, D. G., Zehr, J. P., Paerl, H. W., Bergman, B., & Carpenter, E. J. (1997), *Trichodesmium*, a  
403 globally significant marine cyanobacterium, *Science*, 276(5316), 1221-1229,  
404 <https://doi.org/10.1126/science.276.5316.1221>
- 405 Dore, J. E., Letelier, R. M., Church, M. J., Lukas, R., & Karl, D. M. (2008), Summer phytoplankton  
406 blooms in the oligotrophic North Pacific Subtropical Gyre: Historical perspective and recent  
407 observations, *Prog. Oceanogr.*, 76(1), 2-38, <https://doi.org/10.1016/j.pocean.2007.10.002>
- 408 Doty, M. S., & Oguri, M. (1956), The island mass effect, *J. Cons. Int. Explor. Mer.*, 22(1), 33-37,  
409 <https://doi.org/10.1093/icesjms/22.1.33>
- 410 Gove, J. M., McManus, M. A., Neuheimer, A. B., Polovina, J. J., Drazen, J. C., Smith, C. R., et al.  
411 (2016), Near-island biological hotspots in barren ocean basins, *Nat. Commun.*, 7, 10581,  
412 <https://doi.org/10.1038/ncomms10581>

- 413 Guieu, C., Bonnet, S., Petrenko, A., Menkes, C., Chavagnac, V., Desboeufs, C., Maes, C., & Moutin, T.  
 414 (2018), Iron from a submarine source impacts the productive layer of the Western Tropical South  
 415 Pacific (WTSP), *Sci. Rep.*, 8, <https://doi.org/10.1038/s41598-018-27407-z>
- 416 Hasegawa, D., Lewis, M. R., & Gangopadhyay, A. (2009), How islands cause phytoplankton to bloom in  
 417 their wakes, *Geophys. Res. Lett.*, 36, L20605, <https://doi.org/10.1029/2009GL039743>
- 418 Huffman, G. J., Stocker, E. F., Bolvin, D. T., Nelkin, E. J., & Tan, J. (2019), GPM IMERG Final  
 419 Precipitation L3 1 day 0.1 degree x 0.1 degree V06, Edited by Andrey Savtchenko, Greenbelt, MD,  
 420 Goddard Earth Sciences Data and Information Services Center (GES DISC), Accessed: 05/27/2019,  
 421 doi:10.5067/GPM/IMERGDF/DAY/06
- 422 Johnson, K. S., Riser, S. C., & Karl, D. M. (2010), Nitrate supply from deep to near-surface waters of the  
 423 North Pacific subtropical gyre, *Nature*, 465, 1062-1065, <https://doi.org/10.1038/nature09170>
- 424 Lehahn, Y., Koren, I., Sharoni, S., d'Ovidio, F., Vardi, A., & Boss, E. (2017), Dispersion/dilution  
 425 enhances phytoplankton blooms in low-nutrient waters, *Nat. Commun.*, 8, 14868,  
 426 <https://doi.org/10.1038/ncomms14868>
- 427 Mahadevan, A. (2016), The impact of submesoscale physics on primary productivity of plankton, *Ann.*  
 428 *Rev. Mar. Sci.*, 8(1), 161-184, <https://doi.org/10.1146/annurev-marine-010814-015912>
- 429 Martinez, E., & Maamaatuaiahutapu, K. (2004), Island mass effect in the Marquesas Islands: Time  
 430 variation, *Geophys. Res. Lett.*, 31(18), <https://doi.org/10.1029/2004gl020682>
- 431 McGillicuddy, D. J. J., Laurence, A. A., Bates, N. R., Bibby, T., Buesseler, K. O., Carlson, C. A., et al.  
 432 (2007), Eddy/wind interactions stimulate extraordinary mid-ocean plankton blooms, *Science*,  
 433 316(5827), 1021-1026, <https://doi.org/10.1126/science.1136256>
- 434 Menkes, C. E., Lengaigne, M., Lévy, M., Ethé, C., Bopp, L., Aumont, O., et al. (2016), Global impact of  
 435 tropical cyclones on primary production, *Global Biogeochem. Cycles*, 30(5), 767-786,  
 436 <https://doi.org/10.1002/2015gb005214>
- 437 Messié, M., & Chavez, F. P. (2017), Nutrient supply, surface currents, and plankton dynamics predict  
 438 zooplankton hotspots in coastal upwelling systems, *Geophys. Res. Lett.*, 44(17), 8979-8986,  
 439 <https://doi.org/10.1002/2017GL074322>
- 440 Messié, M., Radenac, M.-H., Lefèvre, J. & Marchesiello, P. (2006), Chlorophyll bloom in the western  
 441 Pacific at the end of the 1997-98 El Niño: the role of the Kiribati Islands, *Geophys. Res. Lett.*, 33,  
 442 L14601, <https://doi.org/10.1029/2006GL026033>
- 443 Moosdorf, N., Stieglitz, T., Waska, H., Dürr, H. H., & Hartmann, J. (2015), Submarine groundwater  
 444 discharge from tropical islands: a review, *Grundwasser*, 20(1), 53-67, <https://doi.org/10.1007/s00767-014-0275-3>
- 446 Moutin, T., Doglioli, A. M., de Verneil, A., & Bonnet, S. (2017), Preface: The Oligotrophy to the Utra-  
 447 oligotrophy PACific Experiment (OUTPACE cruise, 18 February to 3 April 2015), *Biogeosciences*,  
 448 14(13), 3207-3220, <https://doi.org/10.5194/bg-14-3207-2017>
- 449 Moutin, T., Karl, D. M., Duhamel, S., Rimmelin, P., Raimbault, P., Van Mooy, B. A. S., & Claustre, H.  
 450 (2008), Phosphate availability and the ultimate control of new nitrogen input by nitrogen fixation in  
 451 the tropical Pacific Ocean, *Biogeosciences*, 5(1), 95-109, <https://doi.org/10.5194/bg-5-95-2008>
- 452 Moutin, T., Wagener, T., Caffin, M., Fumenia, A., Gimenez, A., Baklouti, M., et al. (2018), Nutrient  
 453 availability and the ultimate control of the biological carbon pump in the western tropical South  
 454 Pacific Ocean, *Biogeosciences*, 15(9), 2961-2989, <https://doi.org/10.5194/bg-15-2961-2018>
- 455 Palacios, D. M. (2002), Factors influencing the island-mass effect of the Galapagos archipelago, *Geophys.*  
 456 *Res. Lett.*, 29(23), 2134, <https://doi.org/10.1029/2002GL016232>

- 457 Raapoto, H., Martinez, E., Petrenko, A. A., Doglioli, A. M., Gorgues, T., Sauzède, R., et al. (2019), Role  
 458 of iron in the remarkable Marquesas island mass effect, *J. Geophys. Res. Oceans*, in press,  
 459 <https://doi.org/10.1029/2019JC015275>
- 460 Rousselet, L., de Verneil, A., Doglioli, A. M., Petrenko, A. A., Duhamel, S., Maes, C., & Blanke, B.  
 461 (2018), Large- to submesoscale surface circulation and its implications on biogeochemical/biological  
 462 horizontal distributions during the OUTPACE cruise (southwest Pacific), *Biogeosciences*, *15*(8), 2411-  
 463 2431, <https://doi.org/10.5194/bg-15-2411-2018>
- 464 Ryan, P. R., Polito, P. S., Strutton, P. G., & Chavez, F. P. (2002), Unusual large-scale phytoplankton  
 465 blooms in the equatorial Pacific, *Prog. Oceanogr.*, *55*(3-4), 263-285, [https://doi.org/10.1016/S0079-6611\(02\)00137-4](https://doi.org/10.1016/S0079-6611(02)00137-4)
- 467 Shiozaki, T., Kodama, T., & Furuya, K. (2014), Large-scale impact of the island mass effect through  
 468 nitrogen fixation in the western South Pacific Ocean, *Geophys. Res. Lett.*, *41*(8), 2907-2913,  
 469 <https://doi.org/10.1002/2014GL059835>
- 470 Signorini, S. C., McClain, C. R., & Dandonneau, Y. (1999), Mixing and phytoplankton bloom in the  
 471 wake of the Marquesas Islands, *Geophys. Res. Lett.*, *26*(20), 3121-3124,  
 472 <https://doi.org/10.1029/1999GL010470>
- 473 Spungin, D., Belkin, N., Foster, R. A., Stenegren, M., Caputo, A., Pujo-Pay, M., et al. (2018),  
 474 Programmed cell death in diazotrophs and the fate of organic matter in the western tropical South  
 475 Pacific Ocean during the OUTPACE cruise, *Biogeosciences*, *15*(12), 3893-3908,  
 476 <https://doi.org/10.5194/bg-15-3893-2018>
- 477 de Verneil, A., Rousselet, L., Doglioli, A. M., Petrenko, A. A., & Moutin, T. (2017), The fate of a  
 478 southwest Pacific bloom: gauging the impact of submesoscale vs. mesoscale circulation on biological  
 479 gradients in the subtropics, *Biogeosciences*, *14*(14), 3471-3486, <https://doi.org/10.5194/bg-14-3471-2017>
- 481 Wilson, C., & Qiu, X. (2008), Global distribution of summer chlorophyll blooms in the oligotrophic  
 482 gyres, *Prog. Oceanogr.*, *78*(2), 107-134, <https://doi.org/10.1016/j.pocean.2008.05.002>
- 483 Wilson, C., Villareal, T. A., Maximenko, N., Bograd, S. J., Montoya, J. P., & Schoenbaechler, C. A.  
 484 (2008), Biological and physical forcings of late summer chlorophyll blooms at 30N in the oligotrophic  
 485 Pacific, *J. Mar. Syst.*, *69*(3-4), 164-176, <https://doi.org/10.1016/j.jmarsys.2005.09.018>
- 486